

MF-NeRF: Memory Efficient NeRF with Mixed-Feature Hash Table

Yongjae Lee, Li Yang, and Deliang Fan

School of Electrical, Computer and Energy Engineering, Arizona State University
Tempe, AZ, United States

yongjae@asu.edu, lyang166@asu.edu, dfan@asu.edu

Abstract

Neural radiance field (NeRF) has shown remarkable performance in generating photo-realistic novel views. Since the emergence of NeRF, many studies have been conducted, among which managing features with explicit structures such as grids has achieved exceptionally fast training by reducing the complexity of multilayer perceptron (MLP) networks. However, storing features in dense grids requires significantly large memory space, which leads to memory bottleneck in computer systems and thus large training time. To address this issue, in this work, we propose MF-NeRF, a memory-efficient NeRF framework that employs a mixed-feature hash table to improve memory efficiency and reduce training time while maintaining reconstruction quality. We first design a mixed-feature hash table to adaptively mix part of multi-level feature grids into one and map it to a single hash table. Following that, in order to obtain the correct index of a grid point, we further design an index transformation method that transforms indices of an arbitrary level grid to those of a canonical grid. Extensive experiments benchmarking with state-of-the-art Instant-NGP, TensorRF, and DVGO, indicate our MF-NeRF could achieve the fastest training time on the same GPU hardware with similar or even higher reconstruction quality. Source code is available at <https://github.com/nfyfamr/MF-NeRF>.

1. Introduction

Representing 3D scenes has garnered significant recognition in various industries. In the past, the conventional method involved breaking down free surfaces into primitive triangles, also known as polygons. However, this approach has been proven to be costly, so it often simplifies the scene to reduce cost which sacrifices the reconstruction quality. Recently, the developments of machine learning have brought new possibilities for scene representation [25, 27]. Notably, the neural radiance field (NeRF) [23] has made a significant advancement in both the quality and effi-

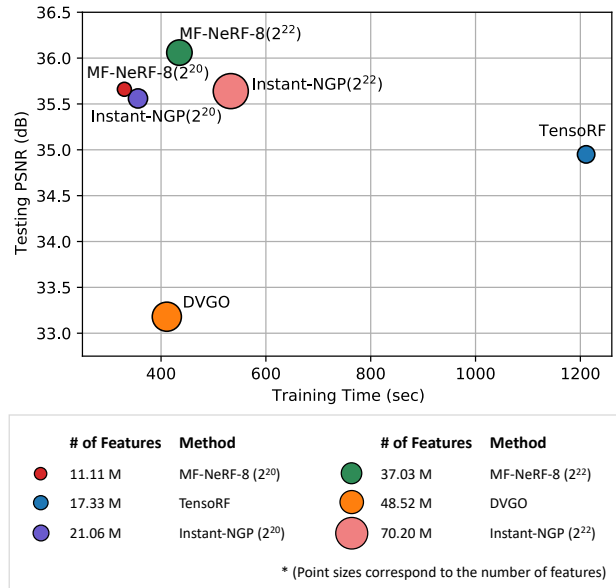


Figure 1. Training time and test results were compared across models, with marker size representing the number of features required for learning a Mic scene [23] (smaller circle is better). The MF-NeRF framework demonstrated impressive efficiency in rapidly learning scenes, achieving this with only half the number of parameters required by our base model, Instant-NGP [24], and in a shorter amount of time.

ciency of synthesizing novel views, which learns a 3D scene by training multi-layer perceptrons (MLPs).

In general, NeRF has two main research directions: implicit and explicit representations. In the implicit representation-based methods [7, 21, 33, 9, 38, 4], it is crucial to provide inputs of sufficient size to encode high-dimensional and complex radiance fields into MLP networks. As one common approach, the positional encoding [23, 39] method decomposes low-dimensional spatial-directional inputs (x, y, z, θ, ϕ) into a set of high-dimensional frequency parameters, helping MLP networks reproduce complex curves and view-dependent light effects. On the other hand, in order for MLP networks to inter-

pret high-dimensional inputs, they need to be both deep and wide. Additionally, due to the infinite and continuous nature of the space, a multitude of giant MLP network queries are required to learn every direction through every point. As a result, the training time and rendering time are typically very large.

On a different track, other prior works [18, 45, 36, 3, 8] address the issues of MLP complexity by abstracting and managing scenes as features through explicit representation. They mainly utilize a feature grid that can inherently represent spatial information through voxel coordinates, enabling the design of small and efficient MLPs. While these approaches drastically reduce the computing time for learning and rendering, they must control the enormous GPU memory usage necessary for storing the large, dense feature grids. To address such memory bottleneck challenge, feature compression methods have been discussed, such as tensor decomposition [2] and hash encoding [24], to manage vast feature grids while minimizing loss in the scene representation details.

In this paper, following the explicit representation approach, we propose MF-NeRF, which utilizes a novel method called *mixed-feature hash table*, for further compressing feature grids. The mixed-feature hash table collects features from varying-distance neighborhoods around queried three-dimensional (3D) points, using voxel windows of different sizes. This manner of feature collection can be seen as a generalized approach for multiresolution hash tables proposed in [24], which manages multiple grids of different resolutions and compresses them by mapping them into smaller hash tables, while our mixed-feature hash table captures features at specific grid levels by using voxel windows. As is widely known, having more features in the grid needs a larger allocation of memory space for the big hash tables and cache buffering on the computer. If such memory space is much larger than computer cache memory, the training time will increase significantly due to greatly increased cache miss ratio, without corresponding improvements in rendering quality, as shown in the analysis of Instant-NGP with hash table sizes ranging from 2^{20} to 2^{22} in Fig. 1. In real applications, this memory bottleneck issue can arise as a major problem when learning on large scenes, such as buildings [37].

In this work, our MF-NeRF targets to address this issue by proposing a flexible and adaptive feature grid compression method through a mixed-feature hash table, which could significantly compress the conventional multiresolution hash feature encoding, leading to a great reduction in training time while maintaining high rendering quality (e.g., MF-NeRF-8 (2^{22}) outperforms Instant-NGP (2^{22}) on the same GPU in Fig. 1). Throughout this paper, we demonstrate that MF-NeRF outperforms existing methods in terms of both memory efficiency and rendering quality.

We summarize our contributions as follows:

- We propose MF-NeRF, an efficient NeRF framework that aims to reduce the parameter size and training time while keeping the reconstruction quality high. We first design a *mixed-feature hash table* to adaptively mix partial feature grid levels into one hash table. Following that, to obtain the correct index of the corner point in the grid space, we further design an *index transformation* method to transform the original window space into grid space.
- We conduct experiments to benchmark MF-NeRF against state-of-the-art (SOTA) methods such as Instant-NGP, TensorRF, and DVGO. Our MF-NeRF method achieves the fastest training time on the same GPU hardware while maintaining similar or higher rendering quality. For example, compared to Instant-NGP, our MF-NeRF-8(2^{22}) setup achieves around 12% training time reduction on the same GPU with 0.2 higher average PSNR in the synthetic NeRF dataset.

2. Related work

2.1. Neural Scene Representations

Inspired by NeRF [23], many works [17, 1, 10, 44, 34, 26, 13, 5] have been proposed for novel view synthesis tasks. Generally, NeRF [23] encodes a scene into a couple of MLP networks, using multiple posed images. Therefore, having consistency between images is crucial, as NeRF struggles to learn the scene when provided with inaccurate pose information or impaired images. Earlier works such as Deblur-NeRF [19] and PDRF [29] have studied ways to train a clear scene from blurry images. Deblur-NeRF optimizes a separate neural network that generates rays to simulate camera motion and defocus blurs, thereby enabling NeRF to capture and represent deblurred scenes. Similarly, in cases where image noise arises from low-light environments or overheated sensors, PDRF [22] approaches the problem by modeling the noise using color blending, preventing NeRF from learning it. On the other hand, NAN [28] focuses on generating a clean image with the same view from a burst of noisy images that have relatively small camera movement, in contrast to what Deblur-NeRF and PDRF assume. In addition, Ev-NeRF [10] demonstrated NeRF is trainable with event camera data rather than regular posed RGB images.

Methods that leverage scene prior information continue to be an active area of research [15, 26]. NerfingMVS [43] trains a neural network that completes sparse point clouds generated by Structure-from-Motion [31] into dense point clouds to help NeRF better understand the scene with the geometry. DS-NeRF [6] uses sparse point clouds to help learn the density distribution of the scene. MVG-NeRF [26]

utilizes depth maps generated by multi-view stereo [32] and compares them with synthesized depth maps produced by neural rendering methods. On the other hand, iNeRF [44] proposed a localization method that estimates the poses of given images by comparing them with neural-rendered images based on possible poses.

NeRF updates the entire MLP network for a given image set, which means it can learn only one scene at a time. Recent research [41, 40, 11] has proved that transformers [39] can be employed to select images from a given set for synthesizing novel view images, rather than directly encoding a scene into MLPs. Additionally, considering epipolar geometry constraints can enhance the restoration of view-dependent lighting effects [34].

2.2. Efficient NeRF Rendering Algorithms

To address the slow training and long rendering time of NeRF, recent research has begun to use explicit data structures for storing and accessing features that encode the shape and color information of a scene [18, 20, 8]. NSVF [18] employs an Octree to store optimized scene features. This approach supports the gradual subdivision of voxels and the pruning of empty cells, which allows increased scene resolution and improved rendering quality. DVGO [35] adaptively increases the resolution of the feature grid during training. In contrast, KiloNeRF [30] uses numerous amount of tiny MLPs instead of one large MLP to dramatically reduce rendering time. SNeRG [8] extracts view-dependent and color features from a trained NeRF, bakes them into a 3D texture atlas, and uses a relatively small MLP to synthesize novel views with the baked features. RT-NeRF [16] performs fast rendering by back projecting the feature grid onto the render target image plane instead of using ray marching. Control-NeRF [14] blends feature grids trained on different scenes to selectively render objects across the scenes.

A recent seminal work, Instant-NGP [24], maps multiresolution grids that encode a scene at various levels of abstraction onto a relatively small memory space using a hash function, allowing for the rapid learning of a plausible scene in seconds. In contrast, TensorRF [2] decomposes a deep feature grid into vectors and matrices, resulting in improved storage efficiency.

2.3. Scene representation of neural radiance field

NeRF [23] uses MLP networks to learn the radiance field of arbitrary scenes. Once sufficiently optimized, NeRF can estimate both the volume density σ and RGB color \mathbf{c} of the continuous function that describes the radiance field. It is then able to reconstruct a photo-realistic view from an unseen pose using a differentiable volume rendering method.

Given a camera pose and pixel coordinates, NeRF generates a camera ray $\mathbf{r}(t) = \mathbf{o} + t\mathbf{d}$ that marches from $\mathbf{o} \in \mathbb{R}^3$

in direction $\mathbf{d} \in [-\pi, \pi]^2$ to the pixel and samples a number of points along the ray \mathbf{r} with a certain distribution. Each sampled point $\mathbf{x} \in \mathbb{R}^3$ is given as input to the MLP $F_\Phi : (\mathbf{x}, \mathbf{d}) \mapsto (\sigma, \mathbf{c})$, and the MLP infers the density $\sigma \in \mathbb{R}$ of the point \mathbf{x} and its RGB color $\mathbf{c} \in \mathbb{R}^3$ corresponding to the ray direction \mathbf{d} . The final color $\hat{C}(\mathbf{r})$ for the ray \mathbf{r} (i.e., the color of the pixel) is determined by a weighted sum of the colors of the N sampled points along the ray \mathbf{r} , taking into account the density σ_i and light transmittance T_i of each point \mathbf{x}_i :

$$\begin{aligned}\hat{C}(\mathbf{r}) &= \sum_{i=1}^N T_i (1 - \exp(-\sigma_i \delta_i)) \mathbf{c}_i, \\ T_i &= \prod_{j<i} \exp(-\sigma_j \delta_j),\end{aligned}\tag{1}$$

where δ_i is the distance between consecutive sampled points \mathbf{x}_i and \mathbf{x}_{i+1} , and i and j indicate the order of the sampled points.

3. Method

In this section, we introduce *MF-NeRF*, a flexible framework that encodes a 3D scene in a few compressed feature grids. Fig. 2 illustrates the key concept of MF-NeRF. To begin with, we present a review of multiresolution hash encoding, which is the base architecture of MF-NeRF, in Sec. 3.1. Then, we describe the mixed-feature hash table and voxel window in Sec. 3.2.1, followed by the index transformation of the window to the grid space in Sec. 3.2.2. At last, we cover our training process and loss setting in Sec. 3.2.3.

3.1. Preliminary

Multiresolution hash encoding To improve training efficiency while keeping reconstruction quality, prior NeRF methods [35, 20, 18, 24] encode the information of each small space in a voxel by dividing the 3D space into unit cubes, rather than training the entire scene on a large MLP. This approach largely reduces training time since only the scene features contained in the adjacent eight grid points need to be updated, instead of the entire weight of the MLP network.

Instant-NGP [24], as a representative work in this field, compresses multiple feature grids with different resolutions into separate hash tables for expressing smoothness and minimizing worthless grid points. Specifically, it owns two types of trainable parameters: encoding parameters (scene features) Θ for hash tables and weight parameters Φ for the MLP network. The encoding parameters are arranged into L levels of grids with varying resolutions, where each corner point in the grids contains a feature vector of size F , and every feature vector of each grid is stored in the corresponding hash table of maximum size T at the l -th level.

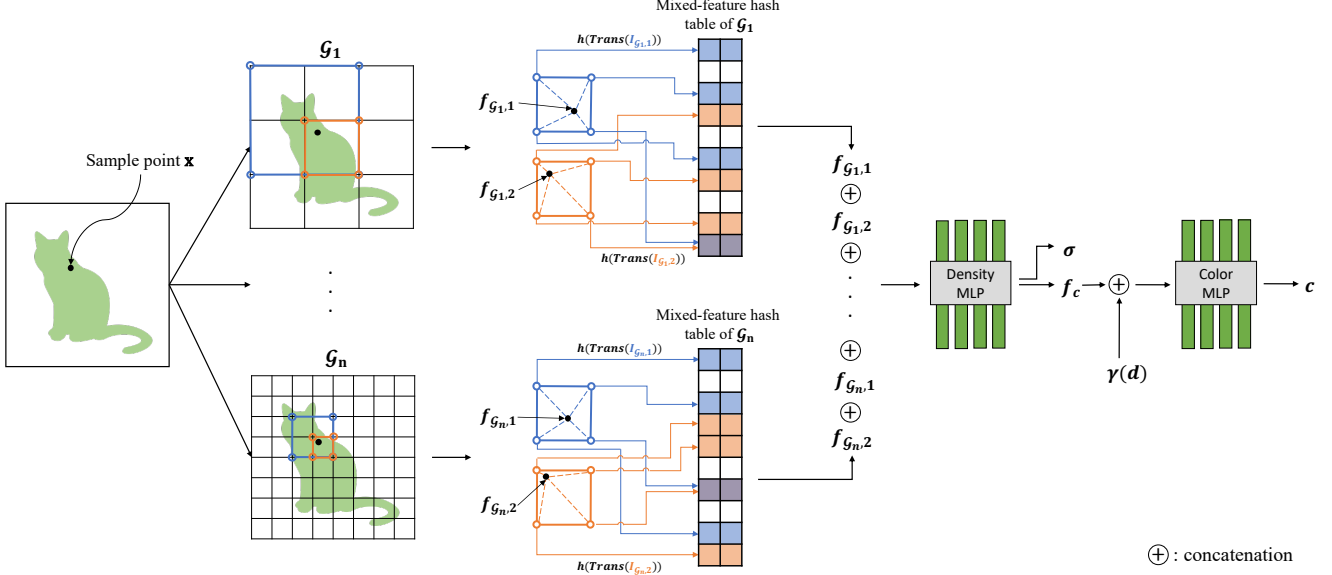


Figure 2. **Overview of MF-NeRF in 2D representation.** Given a sampled point \mathbf{x} , we find corner indices $\mathbf{I}_{\mathcal{G}_i,j}$ of voxel windows of different sizes that surround the point in each feature grid. To retrieve the feature vectors in the hash table, we conduct an index transformation that maps indices in window space to grid space. After linearly interpolating and concatenating the feature vectors, we feed the resulting interpolated feature vectors $f_{\mathcal{G}_i,j}$, along with the positional embedded viewing direction $\gamma(\mathbf{d})$ into MLPs to estimate the density σ and color \mathbf{c} of the point. This method could be simply extended to three dimensions as well.

The resolution ratio b between consecutive grids is defined as follows:

$$b = (N_{max}/N_{min})^{1/(L-1)}, \quad (2)$$

where N_{max} and N_{min} are the maximum resolution and minimum resolution of grids, respectively. Hence, the resolution of l -th grid is given by:

$$N_l = \lfloor N_{min} \cdot b^{l-1} \rfloor \quad (3)$$

Given a sampled point \mathbf{x} and a viewing direction \mathbf{d} , Instant-NGP locates the grid indices $\mathbf{I}_{\mathcal{G}_l} = (i, j, k)$ of the eight corner points that surround the sampled point \mathbf{x} in each of the grids \mathcal{G}_l , resulting in a total of $8 \cdot L$ corner point indices. Then, the spatial hash $h(\cdot)$ [26] is used for each $\mathbf{I}_{\mathcal{G}_l}$ to obtain the index in the associated hash table θ_l , which can be formulated as:

$$h(\mathbf{I}_{\mathcal{G}_l}) = (i \cdot \pi_1 \oplus j \cdot \pi_2 \oplus k \cdot \pi_3) \bmod T, \quad (4)$$

where \oplus is bit-wise XOR operator, T is the hash table maximum size, and π is prime number (i.e., $\pi_1 = 1$, $\pi_2 = 2,654,435,761$, and $\pi_3 = 805,459,861$). After that, the eight F -dimensional feature vectors of eight corner points retrieved from l -th hash table θ_l are trilinearly interpolated resulting in $f_{\mathcal{G}_l} \in \mathbb{R}^F$. Then, the L feature vectors are concatenated into $\mathbf{y} = [f_{\mathcal{G}_1}; \dots; f_{\mathcal{G}_L}]$, which serves as the input to the MLP, with viewing direction \mathbf{d} . The MLP is constructed by a density MLP m_d and a color MLP m_c

which are parameterized by Φ_d and Φ_c (i.e., $\Phi = [\Phi_d; \Phi_c]$), respectively. The first output element of m_d is used as the density value σ :

$$\sigma = m_d(\mathbf{y}; \Phi_d)[0], \quad \mathbf{c} = m_c(m_d(\mathbf{y}), \mathbf{d}; \Phi_c) \quad (5)$$

Limitations of multiresolution hash encoding However, although the multiresolution hash encoding enables fast learning speed compared to conventional NeRF [23], there still remain several limitations. First, it inefficiently uses dense trainable feature grids to represent wide empty spaces and smooth surfaces that inherently exist in 3D space, neglecting the redundancy of these feature grids. Second, multiresolution hash encoding compresses features into multiple hash tables corresponding to feature grids of different resolutions via hash function, which means it still has to manage as many as L feature grids. Because T and L crucially affect the learning capacity of Instant-NGP, higher values are needed for reconstructing high-quality scenes with more details. Thus, it inevitably suffers from large encoding parameter size, which is orders of magnitude larger than the weight parameters of the MLP. For instance, in a general setting of Instant-NGP with a hash table size T of 2^{19} and feature resolution levels L of 16, the resulting encoding parameter size is 12.6 M, which is **1,191** \times larger than the weight parameter size (10k). This memory issue can cause a high computer cache miss ratio and become a bottleneck in training, especially when T becomes larger,

which is also discussed in the Instant-NGP work [24]. Correspondingly, it may constrain its real-world application, for example, on large-scale view synthesis or memory-limited edge device deployment.

3.2. MF-NeRF

In this section, we present MF-NeRF, a NeRF framework that is designed to maintain reconstruction quality while reducing parameter size and training time through memory-efficient techniques. As illustrated in Fig. 2, we first design a **mixed-feature hash table** to adaptively mix partial feature grids into one hash table. Following that, to obtain the correct index of the corner point in the grid space, we further design an **index transformation** method that transforms an index in window space into grid space. After linearly interpolating the eight corner point features, we feed them into a sequence of MLPs to estimate the density and color values of the queried point. The detailed techniques will be introduced in the following sections.

3.2.1 Mixed-Feature Hash Table

The multiresolution hash encoding requires the same number of hash tables as the feature grid resolution levels (e.g., 16), resulting in a large encoding parameter size. To address this issue, we propose a mixed-feature hash table approach, in which partial of the feature grids can adaptively mix features while sharing one hash table. By doing so, the number of required hash tables is reduced, which leads to a reduction in the encoding parameter size. Furthermore, such mixed-feature hash table mimics the acquisition of a feature vector from a grid with missing resolution by using a voxel window instead of a large number of grids, which helps to avoid loss of features due to a decreasing number of hash tables. Moreover, in our method, the mixed-feature granularity is a hyperparameter, which allows for optimization of the number of hash tables based on the target hardware memory budget, parameter size, and reconstruction quality.

Specifically, we first construct G grids $\{\mathcal{G}_i \mid i = 1, \dots, G\}$ and corresponding hash tables, each with a maximum size of T . These feature grids encode scene features at different abstractions and store them in the corresponding hash tables. We further design $W \in \{1, 2, 4, 8, \dots, L\}$ voxel windows to capture more local information at each grid, compensating for missing feature grids. Throughout this paper, we automatically select W using the simple equation $L = G \cdot W$. Therefore, the number of encoding parameters when W is larger than 1 is lower than that of Instant-NGP under the same L option. The resolution ratio b_G between consecutive feature grids and the resolution ratio b_W be-

tween consecutive voxel windows are defined as follows:

$$b_G = (b_W)^W \quad (6)$$

$$b_W = (N_{max}/N_{min})^{1/(G \cdot W - 1)} \quad (7)$$

The co-design of feature grids and voxel windows in our method ensures that the resolution ratio b_W of voxel windows matches the resolution ratio b of feature grids in the original multiresolution hash encoding under the same setting of grid levels L , while providing greater flexibility in optimizing the number of feature grids. That means the mixed-feature hash table method is a more generalized approach to the multiresolution hash encoding. For example, with a fixed L for MF-NeRF and Instant-NGP, when W is 1 (i.e., $G = L$), MF-NeRF works in the same way as the multiresolution hash encoding; However, when W is L (i.e., $G = 1$), MF-NeRF employs a single hash table for all grids.

3.2.2 Index Transformation

The proposed mixed-feature hash table method allows voxel windows and their associated feature grid to share one hash table. Therefore, in order to retrieve the feature vectors for each corner point $\mathbf{I}_{\mathcal{G}_i,j}$ in the j -th voxel window at the i -th grid \mathcal{G}_i , we first need to find the grid point indices $\mathbf{I}_{\mathcal{G}_i,W}$ that are mapped by those corners. To achieve this, we devise an index transformation function $Trans(\cdot)$:

$$\begin{aligned} Trans(\mathbf{I}_{\mathcal{G}_i,j}) &= \lfloor \mathbf{I}_{\mathcal{G}_i,j} * N_{\mathcal{G}_i,W} / N_{\mathcal{G}_i,j} \rfloor \\ &= \mathbf{I}_{\mathcal{G}_i,W}, \end{aligned} \quad (8)$$

where $N_{\mathcal{G}_i,W}$ refers to the resolution of the finest voxel window of grid \mathcal{G}_i , which is identical to the resolution of grid \mathcal{G}_i , and $N_{\mathcal{G}_i,j}$ is the resolution of the j -th voxel window of grid \mathcal{G}_i . By using this, we can obtain the correct index of the corner point in the i -th grid space and query the feature vectors from the i -th hash table θ_i using the hash function $h(\cdot)$.

3.2.3 Training

The proposed MF-NeRF is trained by using a set of posed images in a semi-supervised manner. Specifically, we jointly optimize both encoding and weight parameters by calculating the L2 loss between the rendered pixel color $\hat{C}(\mathbf{r})$ and the ground truth pixel color $C(\mathbf{r})$. The loss function is defined as:

$$Loss = \sum_{\mathbf{r} \in \mathcal{R}} \|\hat{C}(\mathbf{r}) - C(\mathbf{r})\|_2 \quad (9)$$

where \mathcal{R} is a batch of camera rays randomly sampled from all the pixels in the image set.

Overall, the whole training process can be illustrated as follows: given a sampled point \mathbf{x} and a viewing direction \mathbf{d} , MF-NeRF first obtains the indices $\mathbf{I}_{\mathcal{G}_i,j} = (l, m, n)$

of the eight corner points surrounding the point \mathbf{x} in the j -th voxel window space of the i -th feature grid. Before hashing $I_{\mathcal{G}_{i,j}}$, these indices in the voxel window space are transformed to the grid space they belong to by using the $Trans(\cdot)$ function as shown in Eq. 8. After this transformation (i.e., eight $I_{\mathcal{G}_{i,W}}$), the hash function (Eq. 4) is used to retrieve feature vectors from the mixed-feature hash table θ_i . The eight feature vectors corresponding to the eight corner points are then trilinearly interpolated, resulting in one feature vector $f_{\mathcal{G}_{i,j}}$. After iterating for over all combinations of feature grids and voxel windows, the L interpolated feature vectors are concatenated (i.e., $\mathbf{y} = [f_{\mathcal{G}_{1,1}}; \dots; f_{\mathcal{G}_{1,W}}; f_{\mathcal{G}_{2,1}}; \dots; f_{\mathcal{G}_{G,W}}]$, where $L = G \cdot W$) and forwarded to the density MLP m_d and the color MLP m_c along with the viewing direction \mathbf{d} (Eq. 5).

4. Experiments

We first conduct an ablation study to find the optimal configuration balancing between parameter size and reconstruction quality. After that, we extend our comparison with SOTA NeRF variants.

4.1. Experimental setup

Dataset We trained MF-NeRF and the baselines on the popular Synthetic NeRF dataset [23], which includes eight different scenes. Each scene contains 400 posed images, consisting of 100 for training, 100 for validation, and 200 for testing, all at a resolution of 800×800 .

Metric We used three commonly used metrics to evaluate the performance of our method and the baselines: peak signal-to-noise ratio (PSNR), structural similarity index measure (SSIM) [42], and learned perceptual image patch similarity of VGG (LPIPS-VGG) [46]. These metrics quantify the similarity between the ground truth image and the reconstructed image.

Baselines: We consider Instant-NGP [24] as our baseline which uses a multiresolution hash table to encode scene features. Moreover, we also compare to other two SOTA methods: TensoRF [2] and DVGO [35].

Implementation details We adopted Adam [12] optimizer with an initial learning rate of $2 \cdot 10^{-2}$, which decreased to $7.86 \cdot 10^{-4}$ using cosine decay. All the Synthetic scenes were trained with the same hyperparameters, including a batch size of 16384, $N_{max} = 2048$, $N_{min} = 16$, $L = 16$, and $F = 2$, unless otherwise specified. For the Lego scene, training for 20k iterations took approximately 7 minutes on a single NVIDIA Quadro RTX 5000 GPU.

We configured the density MLP with 1 hidden layer and 64 channels, and the color MLP with 2 hidden layers and

Instant-NGP		MF-NeRF-1	
# of Features	PSNR	# of Features	PSNR
3,293,600	34.95	2,097,152	35.06
6,177,184	35.32	4,194,304	35.40
11,445,040	35.66	8,388,608	35.79
21,061,904	35.82	16,777,216	35.85

Table 1. MF-NeRF with a single hash table (MF-NeRF-1) demonstrates that it can learn a scene with smaller memory space usage.

128 channels for each layer. The outputs of both MLPs are activated by LeRU function. Unlike Instant-NGP, we chose wider channels for the color MLP. We believe that larger nodes in a layer help interpret the given features into more plausible colors. We mainly select $G = 8$ by default if not mentioned separately.

4.2. Experimental Results

Scene compression First, we investigate how MF-NeRF can effectively compress a scene. To do this, we train MF-NeRF in the extreme case where there is only one single hash table (i.e., $G = 1$). While keeping the other settings the same, we vary only the hash table size and report the training results. In Tab. 1, we show the results of training Instant-NGP and MF-NeRF-1 ($L = 16$, $G = 1$, $W = 16$) on the Lego scene (both methods have $L = 16$, $F = 2$, $N_{min} = 16$, $N_{max} = 1025$, batch = 16384, iters = 20k settings in common). Interestingly, MF-NeRF achieves better performance than Instant-NGP with 20-36% fewer parameters. We believe this result suggests that Instant-NGP learns similar features among each grid, leading to unnecessary redundancy.

Comparison with Instant-NGP Sharing a single hash table among all windows (i.e., MF-NeRF-1) can significantly reduce memory usage. However, it may also lead to a decline in learning performance due to limited memory space. Therefore, optimizing the number of hash tables that multiple windows should share is crucial. To determine the ideal value for G , we conducted experiments by doubling the number of hash tables from $G = 1$ up to $G = 16$, which corresponds to the optimal value of L used in Instant-NGP. We report the performance of MF-NeRF- G with different G settings of 1, 2, 4, and 8 in Tab. 2. Compared to Instant-NGP, we can see that MF-NeRF-8 achieved a parameter reduction of 47.00%/47.44%/47.23%/45.94%, and training time reductions of 4s/38s/175s/290s, with a 0.09/0.2/0.24/0.18 PSNR improvement at all four different T settings, respectively. In addition, it is interesting to see that as the hyperparameter T increased, MF-NeRF showed larger training time reductions compared to Instant-NGP, indicating that the larger parameters of Instant-NGP are a bottleneck that constrains its training time. Moreover, we found that the PSNR consistently improves with increasing

parameter size when comparing different MF-NeRF- G settings.

and rendering quality with smaller parameter size compared to the prior Instant-NGP method.

Benchmarking with SOTA methods We compared the performance of MF-NeRF with other SOTA methods, including TensorRF [2], DVGO [35], and Instant-NGP [24] using the same eight Synthetic scenes and the same GPU hardware. The comprehensive comparison results are reported in Sec. 4.2. Although TensorRF shows overall high performance, it has the largest training time, with around $3.4\times$ and $2.3\times$ longer training time than our MF-NeRF-8 (2^{20}) and MF-NeRF-8 (2^{22}), respectively. However, the average PSNR difference is only 0.1 and 0.01, respectively. As can be seen, both MF-NeRF-8 (2^{20}) and MF-NeRF-8 (2^{22}) configurations learn the scenes faster and exhibit higher average PSNR and SSIM than DVGO and Instant-NGP. Compared to DVGO, our MF-NeRF-8 (2^{20}) consistently achieves better PSNR and shorter training time on all Synthetic scenes. Specifically, we achieve a 1.22 PSNR improvement and a slight 6s training time reduction on average. In addition, compared to TensorRF, our MF-NeRF-8 (2^{22}) achieves almost the same PSNR (i.e., 0.01 degradation) but significantly reduces the training time by up to $2.4\times$ on average.

4.3. Visualization

Fig. 3 shows a qualitative comparison between NeRF methods on the test data. When comparing the drum surface and legs, it can be observed that MF-NeRF depicts smoother and more accurate shading than Instant-NGP. We can also observe a similar phenomenon in the leaves, which Instant-NGP oddly depicts a dark green color. When considering volume reconstruction, MF-NeRF appears to not miss thin structures. MF-NeRF also recognizes the microphone sensor inside the thin mesh cover in the Mic scene and can depict slender branches without disconnection in the Ficus scene.

5. Conclusion

In this paper, we propose a novel framework for neural radiance field (NeRF) that employs a mixed-feature hash table to improve memory efficiency, reduce training and rendering time, while maintaining reconstruction quality. Previous studies have shown that using explicit data structures for 3D scene features can significantly reduce NeRF’s learning time, but memory constraints have made it challenging to represent fine details. Furthermore, using a high-resolution grid can increase learning time as it requires accessing a wide memory area. To compensate for the lack of details due to a small number of feature grids, MF-NeRF queries features in the mixed-feature hash table at various levels using voxel windows. Our proposed method achieves significant improvements in terms of training time reduction

Lego	# of Features				PSNR				SSIM				LPIPS (VGG)				Training Time			
	2^{20}	2^{21}	2^{22}	2^{23}	2^{20}	2^{21}	2^{22}	2^{23}	2^{20}	2^{21}	2^{22}	2^{23}	2^{20}	2^{21}	2^{22}	2^{23}	2^{20}	2^{21}	2^{22}	2^{23}
Instant-NGP	21.06 M	38.55 M	70.20 M	126.97 M	35.94	35.98	36.01	36.04	.9799	.9808	.9813	.9812	.0208	.0197	.0196	.0192	08:27	11:07	14:23	17:51
MF-NeRF-1	2.10 M	4.19 M	8.39 M	16.78 M	35.31	35.73	36.14	36.18	.9753	.9777	.9796	.9810	.0283	.0240	.0210	.0197	08:03	10:14	11:43	13:06
MF-NeRF-2	4.19 M	7.00 M	11.20 M	19.59 M	35.50	35.83	36.09	36.15	.9767	.9787	.9796	.9809	.0263	.0233	.0212	.0198	08:24	10:20	11:44	13:09
MF-NeRF-4	6.39 M	11.30 M	19.69 M	36.47 M	35.81	36.02	36.18	36.26	.9784	.9797	.9801	.9811	.0230	.0213	.0199	.0187	08:07	10:13	11:46	13:26
MF-NeRF-8	11.16 M	20.26 M	37.04 M	68.64 M	36.03	36.18	36.25	36.22	.9796	.9805	.9812	.9812	.0215	.0202	.0191	.0187	08:23	10:29	12:32	14:59

Table 2. Ablation study varying the number of mixed-feature tables and table sizes. The trailing numbers of MF-NeRF- indicates the number of mixed-feature hash tables G .

Metrics	Methods	Chair	Drums	Ficus	Hotdog	Lego	Materials	Mic	Ship	Avg.
PSNR	TensoRF	35.77	25.93	34.12	37.58	36.59	30.11	34.95	30.71	33.22
	DVGO	34.06	25.40	32.56	36.75	34.67	29.58	33.18	29.02	31.90
	Instant-NGP (2^{20})	35.49	25.78	33.98	37.32	35.92	29.55	35.56	30.37	33.00
	Instant-NGP (2^{22})	35.57	25.88	34.07	37.37	36.05	29.51	<u>35.64</u>	30.29	33.05
	MF-NeRF-8 (2^{20})	<u>35.52</u>	<u>25.91</u>	34.12	<u>37.55</u>	<u>36.07</u>	<u>29.52</u>	35.66	<u>30.62</u>	<u>33.12</u>
	MF-NeRF-8 (2^{22})	<u>35.67</u>	25.92	33.87	37.56	36.28	29.61	36.06	30.68	33.21
SSIM	TensoRF	.9845	.9363	.9827	.9828	.9835	.9523	.9886	.8938	.9630
	DVGO	.9758	.9292	.9774	.9801	.9763	.9503	.9827	.8771	.9561
	Instant-NGP (2^{20})	.9834	<u>.9319</u>	.9819	.9797	.9801	.9456	.9889	<u>.8888</u>	.9600
	Instant-NGP (2^{22})	.9834	.9327	<u>.9822</u>	<u>.9807</u>	<u>.9810</u>	.9455	.9892	.8887	<u>.9604</u>
	MF-NeRF-8 (2^{20})	<u>.9824</u>	.9337	.9823	.9812	.9795	.9453	<u>.9889</u>	<u>.8924</u>	.9607
	MF-NeRF-8 (2^{22})	<u>.9839</u>	.9329	.9818	<u>.9818</u>	<u>.9816</u>	<u>.9470</u>	.9902	.8900	<u>.9612</u>
LPIPS (VGG)	TensoRF	.0219	.0719	.0220	.0304	.0178	.0584	.0146	<u>.1386</u>	.0470
	DVGO	.0276	<u>.0797</u>	<u>.0254</u>	.0336	.0269	<u>.0586</u>	.0177	.1615	.0539
	Instant-NGP (2^{20})	.0225	.0780	.0253	<u>.0378</u>	<u>.0207</u>	.0672	.0167	.1306	<u>.0498</u>
	Instant-NGP (2^{22})	<u>.0217</u>	.0763	.0253	.0349	.0193	.0659	.0163	.1250	.0481
	MF-NeRF-8 (2^{20})	.0233	<u>.0761</u>	<u>.0248</u>	.0338	<u>.0214</u>	.0678	.0167	.1317	.0495
	MF-NeRF-8 (2^{22})	.0207	<u>.0766</u>	<u>.0256</u>	<u>.0326</u>	<u>.0190</u>	.0657	<u>.0151</u>	<u>.1267</u>	<u>.0477</u>
Training Time	TensoRF	23:41	24:27	29:27	<u>29:43</u>	27:13	41:02	20:11	36:54	29:05
	DVGO	07:59	07:54	08:02	09:03	<u>08:33</u>	09:14	06:51	11:02	08:35
	Instant-NGP (2^{20})	<u>07:27</u>	<u>07:04</u>	05:49	10:08	08:34	07:59	<u>05:56</u>	<u>15:42</u>	<u>08:35</u>
	Instant-NGP (2^{22})	12:52	11:20	08:48	17:04	15:46	13:00	08:53	25:45	14:05
	MF-NeRF-8 (2^{20})	07:14	06:50	05:20	<u>09:41</u>	08:30	<u>08:04</u>	05:30	16:41	08:29
	MF-NeRF-8 (2^{22})	10:41	09:47	07:19	14:49	12:36	11:39	07:15	25:13	12:25

Table 3. Quantitative comparison with prior architectures (the numbers in the parentheses of methods indicate the hash table size T)

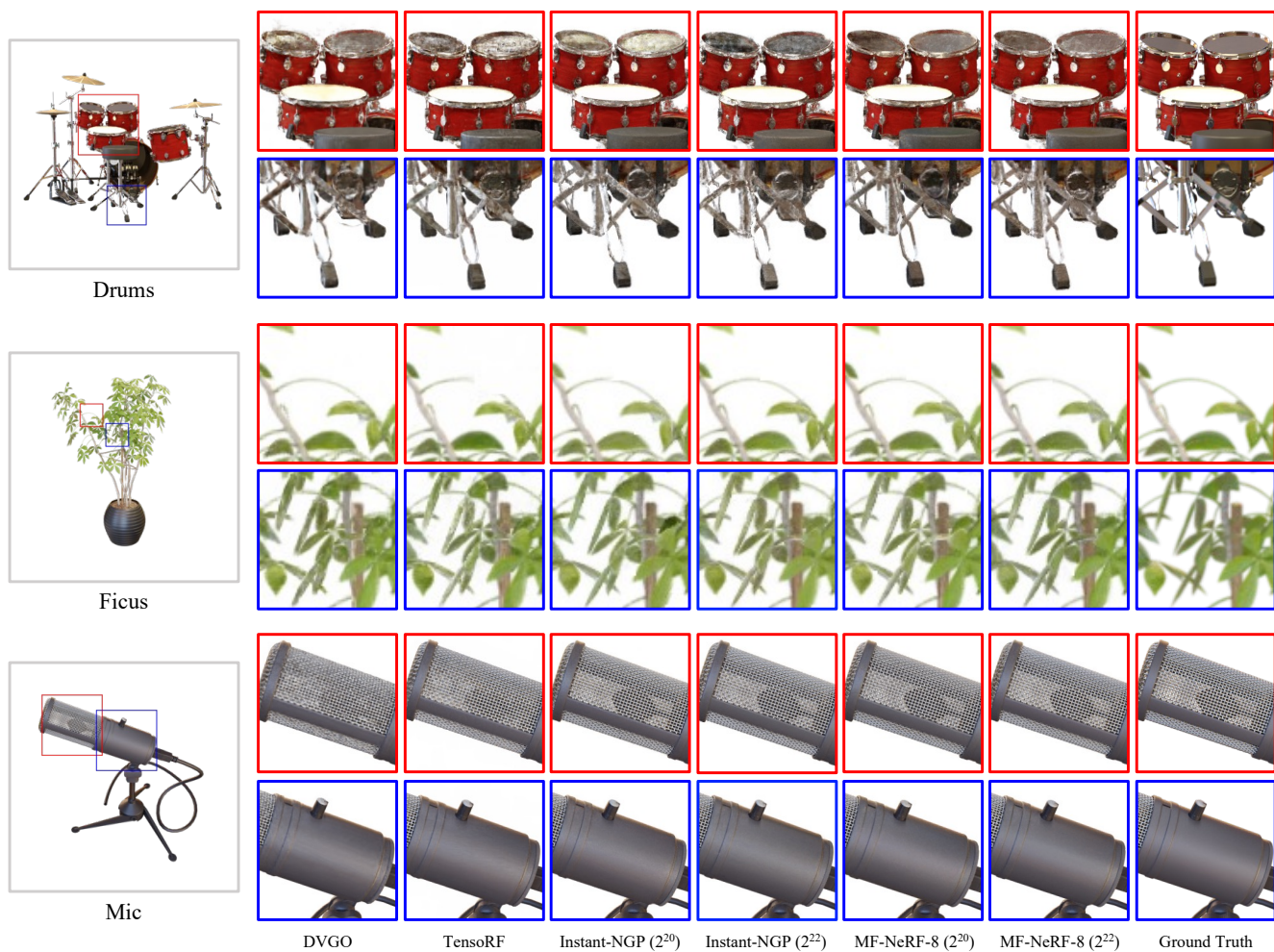


Figure 3. We present qualitative results on three scenes, comparing MF-NeRF with other SOTA methods.

References

- [1] J T Barron, B Mildenhall, M Tancik, P Hedman, R Martin-Brualla, and P P Srinivasan. Mip-NeRF: A Multiscale Representation for Anti-Aliasing Neural Radiance Fields. In *2021 IEEE/CVF International Conference on Computer Vision (ICCV)*, pages 5835–5844, Los Alamitos, CA, USA, 10 2021. IEEE Computer Society. 2
- [2] Anpei Chen, Zexiang Xu, Andreas Geiger, Jingyi Yu, and Hao Su. TensorRF: Tensorial Radiance Fields. In Shai Avidan, Gabriel Brostow, Moustapha Cissé, Giovanni Maria Farinella, and Tal Hassner, editors, *Computer Vision – ECCV 2022*, pages 333–350, Cham, 2022. Springer Nature Switzerland. 2, 3, 6, 7
- [3] Mingfei Chen, Jianfeng Zhang, Xiangyu Xu, Lijuan Liu, Yujun Cai, Jiashi Feng, and Shuicheng Yan. Geometry-Guided Progressive NeRF for Generalizable and Efficient Neural Human Rendering. In Shai Avidan, Gabriel Brostow, Moustapha Cissé, Giovanni Maria Farinella, and Tal Hassner, editors, *Computer Vision – ECCV 2022*, pages 222–239, Cham, 2022. Springer Nature Switzerland. 2
- [4] T Chen, P Wang, Z Fan, and Z Wang. Aug-NeRF: Training Stronger Neural Radiance Fields with Triple-Level Physically-Grounded Augmentations. In *2022 IEEE/CVF Conference on Computer Vision and Pattern Recognition (CVPR)*, pages 15170–15181, Los Alamitos, CA, USA, 6 2022. IEEE Computer Society. 1
- [5] Zhiqin Chen, Thomas Funkhouser, Peter Hedman, and Andrea Tagliasacchi. MobileNeRF: Exploiting the Polygon Rasterization Pipeline for Efficient Neural Field Rendering on Mobile Architectures. pages 1–10. arXiv, 2022. 2
- [6] K Deng, A Liu, J Zhu, and D Ramanan. Depth-supervised NeRF: Fewer Views and Faster Training for Free. In *2022 IEEE/CVF Conference on Computer Vision and Pattern Recognition (CVPR)*, pages 12872–12881, Los Alamitos, CA, USA, 6 2022. IEEE Computer Society. 2
- [7] Mengqi Guo, Chen Li, and Gim Hee Lee. Incremental Learning for Neural Radiance Field with Uncertainty-Filtered Knowledge Distillation. arXiv, 2022. 1
- [8] Peter Hedman, Pratul P Srinivasan, Ben Mildenhall, Jonathan T Barron, and Paul Debevec. Baking Neural Radiance Fields for Real-Time View Synthesis. In *Proceedings of the IEEE/CVF International Conference on Computer Vision (ICCV)*, pages 5875–5884, 10 2021. 2, 3
- [9] Y Hong, B Peng, H Xiao, L Liu, and J Zhang. Head-NeRF: A Realtime NeRF-based Parametric Head Model. In *2022 IEEE/CVF Conference on Computer Vision and Pattern Recognition (CVPR)*, pages 20342–20352, Los Alamitos, CA, USA, 6 2022. IEEE Computer Society. 1
- [10] Inwoo Hwang, Junho Kim, and Young Min Kim. Ev-NeRF: Event Based Neural Radiance Field. In *2023 IEEE/CVF Winter Conference on Applications of Computer Vision (WACV)*, pages 837–847. IEEE, 2023. 2
- [11] M Johari, Y Lepoittevin, and F Fleuret. GeoNeRF: Generalizing NeRF with Geometry Priors. In *2022 IEEE/CVF Conference on Computer Vision and Pattern Recognition (CVPR)*, pages 18344–18347, Los Alamitos, CA, USA, 6 2022. IEEE Computer Society. 3
- [12] Diederik P Kingma and Jimmy Ba. Adam: A Method for Stochastic Optimization. arXiv, 2014. 6
- [13] Andreas Kurz, Thomas Neff, Zhaoyang Lv, Michael Zollhöfer, and Markus Steinberger. AdaNeRF: Adaptive Sampling for Real-Time Rendering of Neural Radiance Fields. In Shai Avidan, Gabriel Brostow, Moustapha Cissé, Giovanni Maria Farinella, and Tal Hassner, editors, *Computer Vision – ECCV 2022*, pages 254–270, Cham, 2022. Springer Nature Switzerland. 2
- [14] Verica Lazova, Vladimir Guзов, Kyle Olszewski, Sergey Tulyakov, and Gerard Pons-Moll. Control-NeRF: Editable Feature Volumes for Scene Rendering and Manipulation. In *Proceedings of the IEEE/CVF Winter Conference on Applications of Computer Vision (WACV)*, pages 4340–4350, 1 2023. 3
- [15] Dongwoo Lee and Kyoung Mu Lee. Dense Depth-Guided Generalizable NeRF. *IEEE Signal Processing Letters*, 30:75–79, 2023. 2

- [16] Chaojian Li, Sixu Li, Yang Zhao, Wenbo Zhu, and Yingyan Lin. RT-NeRF: Real-Time On-Device Neural Radiance Fields Towards Immersive AR/VR Rendering. In *Proceedings of the 41st IEEE/ACM International Conference on Computer-Aided Design, ICCAD '22*, New York, NY, USA, 2022. Association for Computing Machinery. [3](#)
- [17] C Lin, W Ma, A Torralba, and S Lucey. BARF: Bundle-Adjusting Neural Radiance Fields. In *2021 IEEE/CVF International Conference on Computer Vision (ICCV)*, pages 5721–5731, Los Alamitos, CA, USA, 10 2021. IEEE Computer Society. [2](#)
- [18] Lingjie Liu, Jiatao Gu, Kyaw Zaw Lin, Tat-Seng Chua, and Christian Theobalt. Neural Sparse Voxel Fields. In H Larochelle, M Ranzato, R Hadsell, M F Balcan, and H Lin, editors, *Advances in Neural Information Processing Systems*, volume 33, pages 15651–15663. Curran Associates, Inc., 2020. [2](#), [3](#)
- [19] L Ma, X Li, J Liao, Q Zhang, X Wang, J Wang, and P V Sander. Deblur-NeRF: Neural Radiance Fields from Blurry Images. In *2022 IEEE/CVF Conference on Computer Vision and Pattern Recognition (CVPR)*, pages 12851–12860, Los Alamitos, CA, USA, 6 2022. IEEE Computer Society. [2](#)
- [20] Julien N P Martel, David B Lindell, Connor Z Lin, Eric R Chan, Marco Monteiro, and Gordon Wetzstein. AcorN: Adaptive Coordinate Networks for Neural Scene Representation. *ACM Trans. Graph.*, 40(4), 7 2021. [3](#)
- [21] R Martin-Brualla, N Radwan, M M Sajjadi, J T Barron, A Dosovitskiy, and D Duckworth. NeRF in the Wild: Neural Radiance Fields for Unconstrained Photo Collections. In *2021 IEEE/CVF Conference on Computer Vision and Pattern Recognition (CVPR)*, pages 7206–7215, Los Alamitos, CA, USA, 6 2021. IEEE Computer Society. [1](#)
- [22] B Mildenhall, P Hedman, R Martin-Brualla, P P Srinivasan, and J T Barron. NeRF in the Dark: High Dynamic Range View Synthesis from Noisy Raw Images. In *2022 IEEE/CVF Conference on Computer Vision and Pattern Recognition (CVPR)*, pages 16169–16178, Los Alamitos, CA, USA, 6 2022. IEEE Computer Society. [2](#)
- [23] Ben Mildenhall, Pratul P Srinivasan, Matthew Tancik, Jonathan T Barron, Ravi Ramamoorthi, and Ren Ng. NeRF: Representing Scenes as Neural Radiance Fields for View Synthesis. In Andrea Vedaldi, Horst Bischof, Thomas Brox, and Jan-Michael Frahm, editors, *Computer Vision – ECCV 2020*, pages 405–421, Cham, 2020. Springer International Publishing. [1](#), [2](#), [3](#), [4](#), [6](#)
- [24] Thomas Müller, Alex Evans, Christoph Schied, and Alexander Keller. Instant Neural Graphics Primitives with a Multiresolution Hash Encoding. *ACM Trans. Graph.*, 41(4):102:1–102:15, 7 2022. [1](#), [2](#), [3](#), [5](#), [6](#), [7](#)
- [25] M Niemeyer, L Mescheder, M Oechsle, and A Geiger. Differentiable Volumetric Rendering: Learning Implicit 3D Representations Without 3D Supervision. In *2020 IEEE/CVF Conference on Computer Vision and Pattern Recognition (CVPR)*, pages 3501–3512, Los Alamitos, CA, USA, 6 2020. IEEE Computer Society. [1](#)
- [26] Marco Orsingher, Paolo Zani, Paolo Medici, and Massimo Bertozzi. Learning Neural Radiance Fields from Multi-View Geometry. *arXiv*, 2022. [2](#), [4](#)
- [27] J Park, P Florence, J Straub, R Newcombe, and S Lovegrove. DeepSDF: Learning Continuous Signed Distance Functions for Shape Representation. In *2019 IEEE/CVF Conference on Computer Vision and Pattern Recognition (CVPR)*, pages 165–174, Los Alamitos, CA, USA, 6 2019. IEEE Computer Society. [1](#)
- [28] N Pearl, T Treibitz, and S Korman. NAN: Noise-Aware NeRFs for Burst-Denoising. In *2022 IEEE/CVF Conference on Computer Vision and Pattern Recognition (CVPR)*, pages 12662–12671, Los Alamitos, CA, USA, 6 2022. IEEE Computer Society. [2](#)
- [29] Cheng Peng and Rama Chellappa. PDRF: Progressively Deblurring Radiance Field for Fast and Robust Scene Reconstruction from Blurry Images. *arXiv*, 2022. [2](#)
- [30] C Reiser, S Peng, Y Liao, and A Geiger. KiloNeRF: Speeding up Neural Radiance Fields with Thousands of Tiny MLPs. In *2021 IEEE/CVF International Conference on Computer Vision (ICCV)*, pages 14315–14325, Los Alamitos, CA, USA, 10 2021. IEEE Computer Society. [3](#)
- [31] J L Schonberger and J Frahm. Structure-from-Motion Revisited. In *2016 IEEE Conference on Computer Vision and Pattern Recognition (CVPR)*, pages 4104–4113, Los Alamitos, CA, USA, 6 2016. IEEE Computer Society. [2](#)
- [32] Johannes L Schönberger, Enliang Zheng, Jan-Michael Frahm, and Marc Pollefeys. Pixelwise View Selection for Unstructured Multi-View Stereo. In Bastian Leibe, Jiri Matas, Nicu Sebe, and Max Welling, editors, *Computer Vision – ECCV 2016*, pages 501–518, Cham, 2016. Springer International Publishing. [3](#)
- [33] Katja Schwarz, Yiyi Liao, Michael Niemeyer, and Andreas Geiger. GRAF: Generative Radiance Fields for 3D-Aware Image Synthesis. In *Proceedings of the 34th International Conference on Neural Information Processing Systems, NIPS'20*, pages 20154–20166, Red Hook, NY, USA, 2020. Curran Associates Inc. [1](#)
- [34] M Suhail, C Esteves, L Sigal, and A Makadia. Light Field Neural Rendering. In *2022 IEEE/CVF Conference on Computer Vision and Pattern Recognition (CVPR)*, pages 8259–8269, Los Alamitos, CA, USA, 6 2022. IEEE Computer Society. [2](#), [3](#)
- [35] C Sun, M Sun, and H Chen. Direct Voxel Grid Optimization: Super-fast Convergence for Radiance Fields Reconstruction. In *2022 IEEE/CVF Conference on Computer Vision and Pattern Recognition (CVPR)*, pages 5449–5459, Los Alamitos, CA, USA, 6 2022. IEEE Computer Society. [3](#), [6](#), [7](#)
- [36] T Takikawa, J Litalien, K Yin, K Kreis, C Loop, D Nowrouzezahrai, A Jacobson, M McGuire, and S Fidler. Neural Geometric Level of Detail: Real-time Rendering with Implicit 3D Shapes. In *2021 IEEE/CVF Conference on Computer Vision and Pattern Recognition (CVPR)*, pages 11353–11362, Los Alamitos, CA, USA, 6 2021. IEEE Computer Society. [2](#)
- [37] M Tancik, V Casser, X Yan, S Pradhan, B P Mildenhall, P Srinivasan, J T Barron, and H Kretschmar. Block-NeRF: Scalable Large Scene Neural View Synthesis. In *2022 IEEE/CVF Conference on Computer Vision and Pattern Recognition (CVPR)*, pages 8238–8248, Los Alamitos, CA, USA, 6 2022. IEEE Computer Society. [2](#)

- [38] H Turki, D Ramanan, and M Satyanarayanan. Mega-NeRF: Scalable Construction of Large-Scale NeRFs for Virtual Fly-Throughs. In *2022 IEEE/CVF Conference on Computer Vision and Pattern Recognition (CVPR)*, pages 12912–12921, Los Alamitos, CA, USA, 6 2022. IEEE Computer Society. 1
- [39] Ashish Vaswani, Noam Shazeer, Niki Parmar, Jakob Uszkoreit, Llion Jones, Aidan N Gomez, Łukasz Kaiser, and Illia Polosukhin. Attention is All you Need. In I Guyon, U Von Luxburg, S Bengio, H Wallach, R Fergus, S Vishwanathan, and R Garnett, editors, *Advances in Neural Information Processing Systems*, volume 30 of *NIPS’17*, page 6000–6010. Curran Associates, Inc., 2017. 1, 3
- [40] Dan Wang, Xinrui Cui, Septimiu Salcudean, and Z Jane Wang. Generalizable Neural Radiance Fields for Novel View Synthesis with Transformer. *arXiv*, 2022. 3
- [41] Q Wang, Z Wang, K Genova, P Srinivasan, H Zhou, J T Barron, R Martin-Brualla, N Snavely, and T Funkhouser. IBRNet: Learning Multi-View Image-Based Rendering. In *2021 IEEE/CVF Conference on Computer Vision and Pattern Recognition (CVPR)*, pages 4688–4697, Los Alamitos, CA, USA, 6 2021. IEEE Computer Society. 3
- [42] Zhou Wang, A C Bovik, H R Sheikh, and E P Simoncelli. Image quality assessment: from error visibility to structural similarity. *IEEE Transactions on Image Processing*, 13(4):600–612, 4 2004. 6
- [43] Y Wei, S Liu, Y Rao, W Zhao, J Lu, and J Zhou. Nerfin-gMVS: Guided Optimization of Neural Radiance Fields for Indoor Multi-view Stereo. In *2021 IEEE/CVF International Conference on Computer Vision (ICCV)*, pages 5590–5599, Los Alamitos, CA, USA, 10 2021. IEEE Computer Society. 2
- [44] Lin Yen-Chen, Pete Florence, Jonathan T Barron, Alberto Rodriguez, Phillip Isola, and Tsung-Yi Lin. iNeRF: Inverting Neural Radiance Fields for Pose Estimation. In *2021 IEEE/RSJ International Conference on Intelligent Robots and Systems (IROS)*, pages 1323–1330, 2021. 2, 3
- [45] Alex Yu, Ruilong Li, Matthew Tancik, Hao Li, Ren Ng, and Angjoo Kanazawa. PlenOctrees for Real-time Rendering of Neural Radiance Fields. In *2021 IEEE/CVF International Conference on Computer Vision (ICCV)*, pages 5732–5741. IEEE Computer Society, 10 2021. 2
- [46] R Zhang, P Isola, A A Efros, E Shechtman, and O Wang. The Unreasonable Effectiveness of Deep Features as a Perceptual Metric. In *2018 IEEE/CVF Conference on Computer Vision and Pattern Recognition (CVPR)*, pages 586–595, Los Alamitos, CA, USA, 6 2018. IEEE Computer Society. 6